Analysis of Coplanar Waveguide-to-Coplanar Stripline Transitions

Shau-Gang Mao, *Student Member, IEEE*, Chieh-Tsao Hwang, Ruey-Beei Wu, *Senior Member, IEEE*, and Chun Hsiung Chen, *Fellow, IEEE*

***Abstract*—The coplanar waveguide (CPW)-to-coplanar stripline (CPS) transition is analyzed theoretically and experimentally in this paper. To characterize this transition in the lower frequency band, a simple equivalent-circuit model that consists of uniform and nonuniform transmission lines is established. The elements of this model can all be obtained by the closed-form formulas; hence, this model is suitable for computer-aided-design application. This model is then applied to design and analyze the CPW-to-CPS transitions with various structure parameters. In the higher frequency band, the partially prizm-gridded finite-difference time-domain (FDTD) method is employed to take into account the bond-wire effect as well as the surface-wave leakage and space-wave radiation associated with the transition. In this study, results based on equivalent-circuit model, FDTD simulation, and measurement are compared. Good agreement among these results supports the usefulness of the proposed equivalent-circuit model and also validates the FDTD method. By using the equivalent-circuit model to optimize the transition configuration, the CPW-to-CPS transition with broad bandwidth and low insertion loss may be achieved.**

***Index Terms*—Coplanar stripline, coplanar waveguide, equivalent-circuit model, FDTD method, transitions.**

I. Introduction

TRANSITION structures are employed to transform electromagnetic energy between two different types of transmission lines. To guarantee smooth transition, not only the impedance match, but also the field match should be sustained [1]. Sometimes a transition can attain the field match and/or impedance match only in a narrow frequency band and would exhibit high insertion loss elsewhere. This paper analyzes the coplanar waveguide (CPW)-to-coplanar stripline (CPS) transition proposed by [2], aiming at maximizing the bandwidth and minimizing the insertion loss.

The CPW and CPS, as media for hybrid and monolithic microwave integrated circuits, both have the merits of small dispersion, less sensitivity to substrate thickness, simple realization of short-circuited ends, easy integration of series and shunt active and passive components, and eliminating the need of via holes. With the advent of uniplanar microwave integrated circuits [3], the CPS with balanced configuration offers flexibility in the design of uniplanar circuits such as mixers, antennas [4], and optoelectronic devices [5]. It can also feature better immunity to power supply noise and ground noise than the unbalanced transmission line such as CPW [6]. Consequently, balanced CPS structures are attractive in implementing the RF integrated circuits in portable radio transceivers. However, the research works concerning CPS circuit components are relatively limited and only several CPS discontinuities and components were recently examined [7]–[10]. To fully utilize the advantages of these uniplanar transmission lines, implementation of wide-band and low-loss transitions between CPW and CPS is essential.

Previous investigations on CPW-to-CPS transitions have been reported in the literature [11]–[17]. The transitions, developed by Trifunović [11], with Marchand type and double Y-junction type require large chip sizes for implementation at lower frequency and suffer from limited bandwidth due to the use of quarter-wavelength CPW open stub and CPS short stub. The transition proposed by Ho *et al.* [12], which consists of a parallel slotline radial stub and a sudden change of slotline into CPS, has small insertion loss, but its bandwidth is limited by the imperfect open stub termination. Another transition design is accomplished by connecting the CPW abruptly into a slotline with an unterminated slotline open [13], [14]. The slotline is then gradually transformed into the CPS by tapering the slotline metallization planes. The unterminated slotline open produces a decent broad-band performance, but also generates higher radiation loss [15]. One may also employ the quarter-wavelength transformer in designing a transition [16], [17], but the bandwidth would be quite limited and the step discontinuities must be compensated to avoid higher order mode excitation [18].

In this paper, the CPW-to-CPS transition proposed by [2] and shown in Fig. 1(a) is analyzed theoretically and experimentally. By properly designing the structure to fulfill the field match and impedance match conditions, the transition performance may be improved in the sense of bandwidth and insertion loss. Although other researchers [16],[17] introduced similar structures experimentally, their design and analysis procedures are still demanding. This paper intends to give an approach for designing and analyzing this transition based on a simple equivalent-circuit model and an extended finite-difference time-domain (FDTD) technique [19].

II. Theoretical Modeling

In this paper, the CPW-to-CPS transition structure shown in Fig. 1(a) is investigated in detail. For theoretical modeling,

Manuscript received March 4, 1998. This work was supported by the National Science Council of Taiwan, R.O.C. under Grant NSC 87-2213-E-002-056 and under Grant NSC 88-2213-E-002-055.

The authors are with the Department of Electrical Engineering, National Taiwan University, Taipei, Taiwan 10617, R.O.C.

Publisher Item Identifier S 0018-9480(00)00217-9.

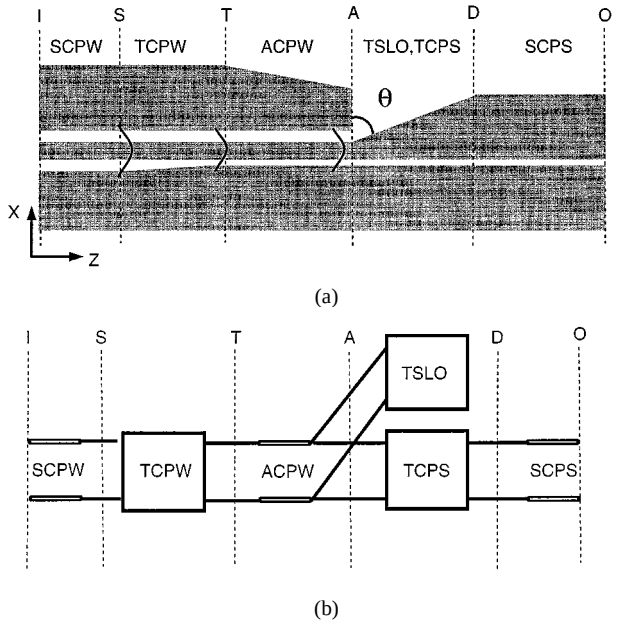

Fig. 1. CPW-to-CPS transition. (a) Physical configuration. (b) Equivalent-circuit model.

this transition structure is decomposed into six parts, i.e., the symmetric coplanar waveguide (SCPW), the asymmetic coplanar waveguide tapered linearly in the lower slot (TCPW), the asymmetric coplanar waveguide tapered linearly in the upper ground plane (ACPW), the unterminated slotline open (TSLO), the asymmetric coplanar stripline tapered linearly in the upper strip (TCPS), and the symmetric coplanar stripline (SCPS). The lower slot width of TCPW is tapered from SCPW to ACPW and then kept the same as the slot width of SCPS so as to minimize the discontinuity effect between them. By narrowing the lower slot width gradually and terminating the open stub on the upper slot, the electromagnetic power on the upper slot may efficiently couple to the lower one. The upper strip of TCPS is also tapered gradually to attain the impedance match between TCPW and SCPS. Typical geometrical dimensions of the CPW-to-CPS transition in Fig. 1(a) are given in Table I.

A. Equivalent-Circuit Model

Fig. 1(b) shows the equivalent-circuit model for the CPW-to-CPS transition in Fig. 1(a). The parts SCPW, ACPW, and SCPS are described by uniform transmission lines for which the characteristic impedance Z (Ω), effective dielectric constant ϵ_{eff}, and attenuation constant α (dB/cm) are determined by the quasi-static formulas based on the conformal mapping technique [20], [21]. Note that the widths of ground planes of SCPW, TCPW, and ACPW are all assumed to be infinite to apply the available formulas. The three tapered structures (TCPW, TCPS, and TSLO) are modeled by nonuniform transmission lines. For theoretical analysis, each nonuniform transmission line is divided into n sections and, in each section, the characteristic impedance is varied linearly and the propagation constant k is assumed to be constant. Let the characteristic impedance profile in the ith section starts with Z_i and varies linearly with slope m_i along the length L_i. The two-port ABCD matrix elements of the ith section can then be given by [22]

$$\begin{aligned}
A_i &= \frac{\pi k}{2m_i}\Big[J_1(u_1)Y_0(u_2) - J_0(u_2)Y_1(u_1)\Big] \\
B_i &= -j\,\frac{\pi k}{2m_i}\,Z_i(1+m_iL_i)\Big[J_1(u_2)Y_1(u_1) - J_1(u_1)Y_1(u_2)\Big] \\
C_i &= j\,\frac{\pi k}{2m_iZ_i}\,\Big[J_0(u_1)Y_0(u_2) - J_0(u_2)Y_0(u_1)\Big] \\
D_i &= -\frac{\pi k}{2m_i}\,(1+m_iL_i)\Big[J_0(u_1)Y_1(u_2) - J_1(u_2)Y_0(u_1)\Big] \quad (1)
\end{aligned}$$

in which $u_1 = k/m_i$, $u_2 = (1+m_iL_i)u_1$, while $J_\rho(x)$ and $Y_\rho(x)$ ($\rho = 0, 1$) denote the ρth-order Bessel functions of first and second kinds, respectively. The $ABCD$ matrices of the nonuniform transmission lines can be evaluated by cascading the $ABCD$ matrices for all sections, i.e.,

$$\begin{bmatrix} A^t & B^t \\ C^t & D^t \end{bmatrix} = \prod_{i=1}^{n} \begin{bmatrix} A_i & B_i \\ C_i & D_i \end{bmatrix}. \quad (2)$$

Expression (2) is very efficient even for large n, although only a few sections (say, $n = 3$) are enough to yield convergent results in most practical cases.

By accounting for the conductor and dielectric losses, the propagation constant k should be regarded as a complex number, i.e., $k = \beta - j\alpha$. In the case of small loss ($\alpha \ll \beta$), the Bessel functions in (1) can be evaluated approximately by [23]

$$\begin{aligned}
B_0(k) &\cong B_0(\beta) + j\alpha B_1(\beta) \\
B_1(k) &\cong B_1(\beta) - j\alpha\left[B_0(\beta) - \frac{B_1(\beta)}{\beta}\right], \qquad B_\rho = J_\rho \text{ or } Y_\rho; \\
&\qquad \rho = 0, 1. \quad (3)
\end{aligned}$$

The S-parameters of TCPW and TCPS are computed by the $ABCD$ matrices in (2). Additional handling is required for the part TSLO, which denotes the aperture radially fanned out from the upper slot of ACPW to the open region with angle θ. This part is basically a nonuniform slotline open whose length ($L_{\text{TSLO}} = 212\,\mu$m) is assumed to be the width of the upper ground plane of ACPW in cross section A of Fig. 1(a). To facilitate numerical analysis, the metallization planes of slotline are assumed to be infinite to apply the available empirical formulas in [20], [24] for the various transmission-line parameters, including the characteristic impedance, effective dielectric constant, and attenuation constant. After obtaining the $ABCD$ matrix of TSLO by (1) and (2), the input impedance seen from the end of ACPW can be given by

$$Z_{\text{in}} = \frac{A^tZ_L + B^t}{C^tZ_L + D^t} \quad (4)$$

in which Z_L denotes the load impedance at the far open end of TSLO. In practice, Z_L can be substituted by an ideal open, i.e., $Z_L = \infty$. Consequently, (4) gives the input impedance of the unterminated slotline open (TSLO) as

$$Z_{\text{in}} = \frac{A^t}{C^t}. \quad (5)$$

TABLE I
DIMENSIONS (ALL IN MICROMETERS) OF CPW-TO-CPS TRANSITION [FIG. 1(a)] FOR FIGS. 2–4 (SUBSTRATE: THICKNESS $h = 635\,\mu$m, $\epsilon_r = 9.8$, $\tan\delta = 0.0001$; METALLIZATION: THICKNESS $t = 3\,\mu$m, $\sigma = 4.1 \times 10^7$ S/m)

	length L	strip width W	slot width S	ground plane width WG
SCPW	508	106.68	48.26	363.22
TCPW	508	106.68	upper 48.26 lower 48.26 - 30.48	upper 363.22 lower 363.22 - 381
ACPW	1016	106.68	upper 48.26 lower 30.48	upper 363.22 - 226 lower 381
TCPS	475	upper 106.68 - 381 lower 381	30.48	——
SCPS	787.4	381	30.48	——

TABLE II
CHARACTERISTIC PARAMETERS OF EQUIVALENT-CIRCUIT MODEL [FIG. 1(b)] FOR FIGS. 2–4

	characteristic impedance Z (Ω)	effective dielectric constant ϵ_{eff}	attenuation constant a (dB/cm)
SCPW	50.5	5.37	1.02
ACPW	47.2	5.38	1.21
SCPS	58.6	4.73	0.73

	input-port impedance Z(0) (Ω)	output-port impedance Z(L) (Ω)	taper length L (μm)	taper subdivision number n
TCPW	50.5	47.2	508	1
TCPS	69.1	58.6	558	1
TSLO	57.5	∞	212	1

TABLE III
DIMENSIONS (ALL IN MICROMETERS) OF CPW-TO-CPS TRANSITION FOR FIG. 7. (SUBSTRATE: THICKNESS $h = 635\,\mu$m, $\epsilon_r = 9.8$, $\tan\delta = 0.0001$; metallization: thickness $t\,\mu$m, $\sigma = 4.1 \times 10^7$ S/m; $Z_{scps} = 65.8\,\Omega$ AND 83.6 Ω)

	length L	strip width W		slot width S	
		65.8 Ω	83.6 Ω	65.8 Ω	83.6 Ω
SCPW	508	142	355	66	172
TCPW	508	142	355	upper 66 lower 66 - 48	upper 172 lower 172 - 155
ACPW	1016	142	355	upper 66 lower 48	upper 172 lower 155
TCPS	158	upper 142 - 363 lower 363	upper 355 - 630 lower 630	48	155
SCPS	787.4	363	630	48	155

The cascade of all uniform and tapered transmission-line parts yields the complete equivalent circuit of the CPW-to-CPS transition, as shown in Fig. 1(b). Notably, the elements of equivalent circuit may all be obtained from the closed-form approximation formulas [20], [21], [24] and, hence, the model can easily be implemented into computer-aided design (CAD) packages. The characteristic parameters of the equivalent-circuit model [Fig. 1(b)], corresponding to Table I, are summarized in Table II.

B. FDTD Method

For a more detailed full-wave analysis, an extended FDTD method [19] is applied to analyze the transition. In this simulation, most of the simulation region is handled by a conventional FDTD algorithm with spatial and time increments of $\triangle = 15.24\,\mu$m and $\triangle_t = 0.0254$ ps, respectively. An extended scheme is employed to deal with the tapered region, which is divided into prizm cells and solved by the finite-element method. Roughly speaking, the whole simulation region is divided into $80 \times 55 \times 260$ cells with eight perfectly matched layers (PML's) [25] located on the outer boundaries. The staircase approximation is used to model the bond wires. In this FDTD simulation, both conductor and dielectric losses are neglected, and the conductor thickness is considered to be zero for simplicity.

To obtain the desired frequency responses, a Gaussian pulse with enough frequency components is used as the incident wave to the transition. By using the fast Fourier transformation, the obtained time-domain data are converted into the frequency-domain ones from which the S-parameters of the transition may be computed.

III. RESULTS AND DISCUSSION

The CPW-to-CPS transition [Fig. 1(a)] with dimensions summarized in Table I is analyzed theoretically and experimentally. All the circuits in this paper are fabricated on a 635-μm-thick alumina substrate ($\epsilon_r = 9.8$ and $\tan\delta = 0.0001$) and have

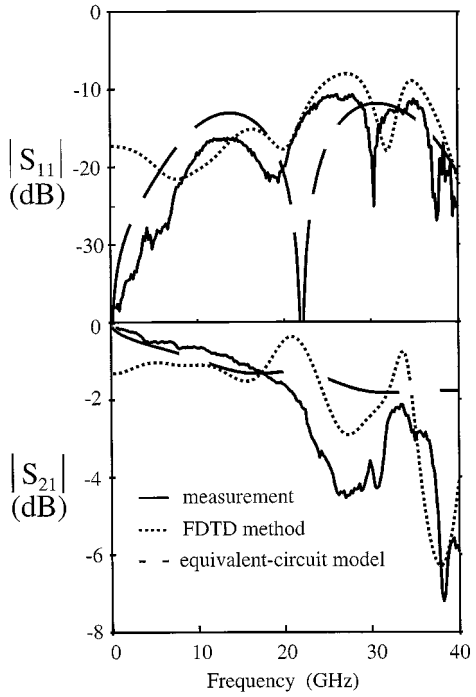

Fig. 2. S-parameters of back-to-back CPW-to-CPS transition configuration ($\theta = 60°$) based on equivalent-circuit model, FDTD method, and measurement. (For Figs. 2–4, the dimensions and characteristic parameters are given in Tables I and II.)

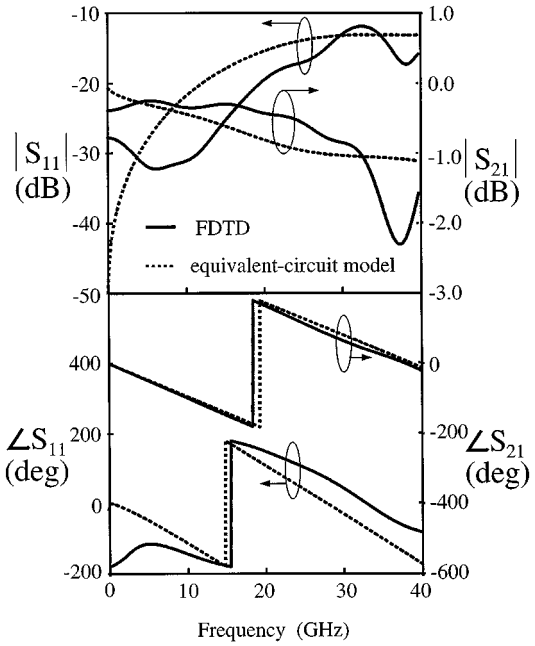

Fig. 3. S-parameters of CPW-to-CPS transition ($\theta = 60°$) based on the equivalent-circuit model and FDTD method.

strips of metallization thickness $t = 3\,\mu$m and conductivity $\sigma = 4.1 \times 10^7$ S/m. The bond wires with length 252.8 μm and diameter 17.7 μm are properly soldered at discontinuities to suppress the non-CPW mode. Theoretically, simulated results are computed based on the equivalent-circuit model [Fig. 1(b)] and the extended FDTD method [19]. The measurements are performed on the back-to-back configuration, using the HP 8510B network analyzer together with the thru-reflection line (TRL) calibration technique. The measurement technique also utilizes on-wafer standards along with a pair of ground–signal–ground RF probes [15].

To examine the applicable frequency range of the equivalent-circuit model, Fig. 2 shows the S-parameters of the back-to-back transition configuration from the cascaded equivalent-circuit model [Fig. 1(b)], FDTD method, and measurement. Agreement among these results supports the usefulness of the proposed equivalent-circuit model and FDTD method. The measured results show that resonances happen near 20 and 30 GHz, which are related to the length of (TCPS + SCPS) and the largest distance between bond wires, respectively. Without taking the bond-wire effect into account, the equivalent-circuit model only presents the first resonance near 20 GHz. This model exhibits better agreement with measurement than FDTD does in the lower frequency band since it has included the conductor and dielectric losses in the simulation. The extended FDTD method is not so reliable in the lower frequency band since it is difficult to span enough simulation region due to memory constraints here. Nonetheless, the extended FDTD method may take into account the surface-wave leakage and space-wave radiation and, hence, its results fit the measured ones better in the higher frequency band. As depicted from the comparison, the applicable frequency range of the proposed equivalent-circuit model is found up to 20 GHz. With the merits of less numerical processing time and easy implementation into CAD software, this model is useful in characterizing the proposed transition configuration. The FDTD analysis, although costing comparatively much more memory and CPU time, becomes necessary and provides useful information for transition design when electromagnetic radiation and coupling effects must be considered.

The CPW-to-CPS transition is useful as a balun in a practical uniplanar circuit, however it should be measured in the back-to-back configuration. By the equivalent-circuit model and the extended FDTD analysis, it is not difficult to characterize the single transition shown in Fig. 1(a). The simulated S-parameters by these two methods are shown in Fig. 3 and reasonable agreement up to 40 GHz between them can be found. It is worthy mentioning that the conductor and dielectric losses are accounted for, but the high frequency surface-wave leakage and space-wave radiation are neglected in the equivalent-circuit model, and vice versa in the extended FDTD method. As a result, the equivalent-circuit model predicts smaller $|S_{21}|$ than FDTD does in the lower frequency range, but larger $|S_{21}|$ as frequency is above 35 GHz.

The energy-transfer mechanism of the CPW-to-CPS transition may be qualitatively discussed by observing the z-directed power densities along the upper slot (P_u) and lower slot (P_l), as shown in Fig. 4. The total electric and magnetic fields are calculated from the FDTD method and the Poynting vectors are integrated along the width of the slots to get the power densities P_u and P_l at the positions of I, S, T, A, D, and O in Fig. 1(a). The input Gaussian power distributions are fed to the upper and lower slots of SCPW at the input port I and kept the same until the plane S. By narrowing the width of the lower slot gradually, the electric field concentrates toward the lower

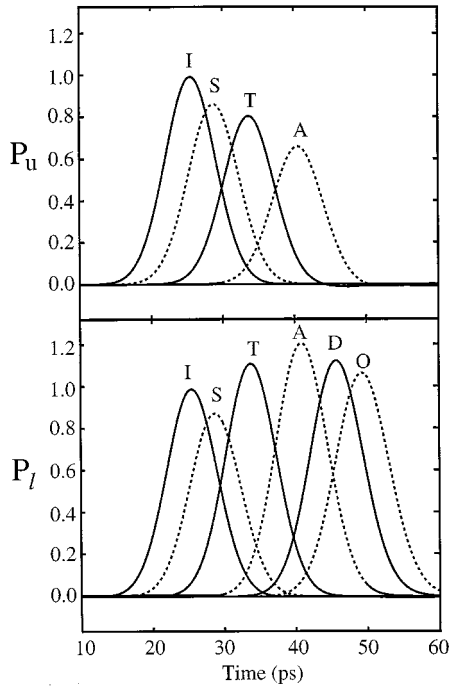

Fig. 4. Gaussian power distributions along the upper and lower slots of CPW-to-CPS transition ($\theta = 60^\circ$).

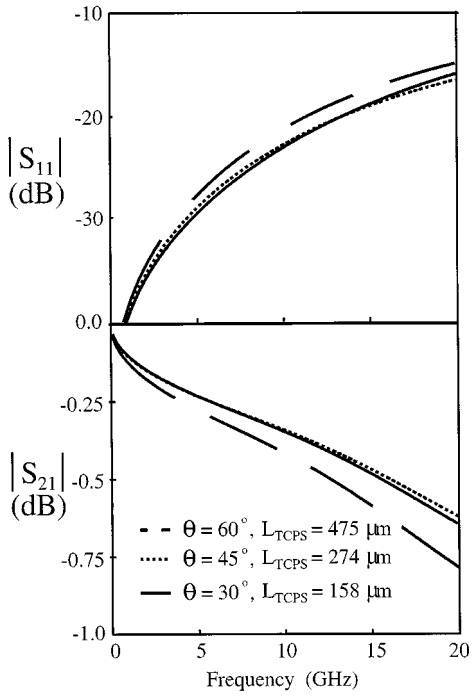

Fig. 5. Simulated S-parameters (by equivalent-circuit model) of CPW-to-CPS transition with inclined angle θ as parameters. (The other dimensions are the same as in Table I.)

slot region, giving $P_u < P_l$ at the plane T. At the exit plane A, the remaining power on the upper slot is partially coupled to the lower one and partially transmitted to the TSLO around which the space-wave radiation loss most likely takes place. Most of the power in the lower slot is transmitted to the balanced SCPS at the output port O through TCPS as shown at planes D and O. By carefully examining the energy-transfer mechanism along the transition, the unterminated slotline open and tapered CPW and CPS structures can be chosen properly so that the transition with small insertion loss may be achieved.

The circuit performance is degraded by the discontinuity mismatch in transition configurations. To reduce this mismatch effect, the inclined angle θ [Fig. 1(a)] associated with the tapered structures TCPS and TSLO is varied to optimize the transition response. Fig. 5 shows the simulated S-parameters of the CPW-to-CPS transition for various inclined angles from the equivalent-circuit model. Quite opposite to our expectation, the case of 60° inclination shows higher $|S_{11}|$ and lower $|S_{21}|$ and is thus less suitable than the 30° case. This demonstrates that the effect of inclined angle is important in determining the transition response. By using the efficient equivalent-circuit model in the design process, the optimum inclined angle for better transition response can easily be achieved in seconds compared to hours in FDTD simulation.

Fig. 6 shows the simulated S-parameters, from the equivalent-circuit model, of the transition with the length of ACPW (L_{ACPW}) as a parameter. It can be found that the reflection coefficient $|S_{11}|$ decreases and the transmission coefficient $|S_{21}|$ increases as the length L_{ACPW} is shortened. Hence, the length L_{ACPW} can be reduced for saving the wafer area if the coupling between TCPW and TCPS is not significant.

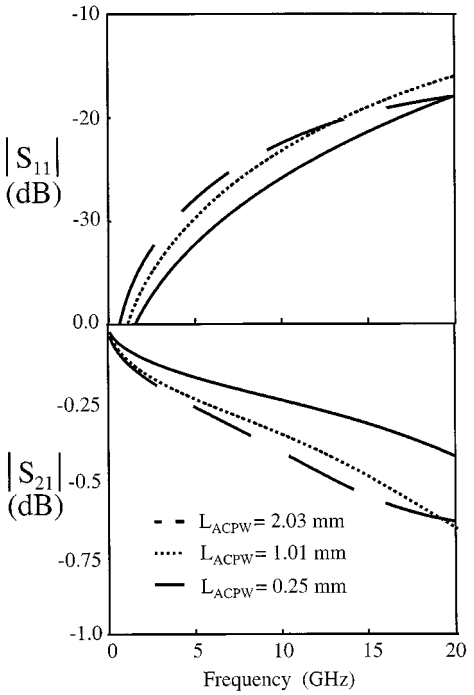

Fig. 6. Simulated S-parameters (by equivalent-circuit model) of CPW-to-CPS transition ($\theta = 30^\circ$, $L_{TCPS} = 158\,\mu$m) with length of ACPW (L_{ACPW}) as parameters. (The other dimensions are the same as in Table I.)

A transition between two media of different impedance levels is sometimes required in practical circuit design. Fig. 7 shows the effect of the impedance of SCPS (Z_{SCPS}) on the S-parameters, which are computed by the equivalent-circuit model with

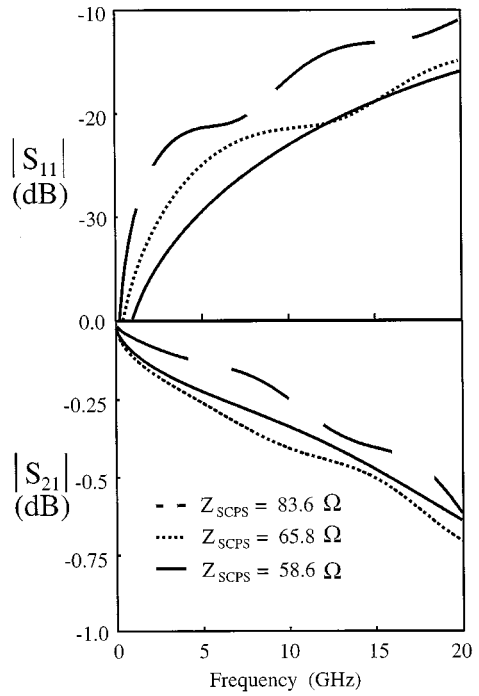

Fig. 7. Simulated S-parameters (by equivalent-circuit model) of CPW-to-CPS transition ($\theta = 30^\circ$, $L_{\mathrm{TCPS}} = 158\ \mu$m) with impedance of SCPS (Z_{SCPS}) as parameters. (For the case $Z_{\mathrm{SCPS}} = 58.6\,\Omega$, the other dimensions are the same as in Table I; and for the cases $Z_{\mathrm{SCPS}} = 63.8$ and $83.6\,\Omega$, the dimensions are shown in Table III.)

$Z_{\mathrm{SCPW}} = 50.5\,\Omega$ in Fig. 1(b). The larger the Z_{SCPS} is, the more the influence of impedance mismatch effect, which results in the larger the value of $|S_{11}|$. However, the transmission coefficient $|S_{21}|$ is varied in a more complicated way: it first decreases and then increases as Z_{SCPS} increases. The transition structure with $Z_{\mathrm{SCPS}} = 83.6\,\Omega$ has larger physical dimensions and, hence, smaller conductor loss of transmission line, making its $|S_{21}|$ value larger than those of the cases with $Z_{\mathrm{SCPS}} = 65.8$ and $58.6\,\Omega$.

IV. Conclusion

In this paper, the CPW-to-CPS transitions for maximizing the bandwidth and minimizing the insertion loss have been analyzed theoretically and experimentally. The transition response has been evaluated numerically using an equivalent-circuit model and extended FDTD method. By considering the leakage and radiation effects in the FDTD method, good agreement between FDTD results and measured ones is observed in the higher frequency band. A simple equivalent-circuit model including conductor and dielectric losses has been established to characterize this transition, and good agreement between these simulated results and measured ones supports the usefulness of the equivalent-circuit model in the lower frequency band. This model, which possesses the merits of less numerical processing time and easy implementation into CAD packages, has been used to examine the transition response by varying the inclined angle θ, the length L_{ACPW}, and the impedance Z_{SCPS} in the lower frequency band. Based on the proposed equivalent-circuit model, the CPW-to-CPS transition configuration may be optimized to achieve broad bandwidth and low insertion loss.

References

[1] J. S. Izadian and S. M. Izadian, *Microwave Transition Design*. Norwood, MA: Artech House, 1988, ch. 1.
[2] H. K. Chiou, C. Y. Chang, and H. H. Lin, "Balun design for uniplanar broad band double balanced mixer," *Electron. Lett.*, vol. 31, pp. 211–212, Nov. 1995.
[3] H. Ogawa and A. Minagawa, "Uniplanar MIC balanced multiplier—A proposed new structure for MIC's," *IEEE Trans. Microwave Theory Tech.*, vol. MTT-35, pp. 1363–1368, Dec. 1987.
[4] K. Tilly, X.-D. Wu, and K. Chang, "Coplanar waveguide fed coplanar strip dipole antenna," *Electron. Lett.*, vol. 30, no. 3, pp. 176–177, Feb. 1994.
[5] J.-H. Son, H.-H. Wang, J. F. Whitaker, and G. A. Mourou, "Picosecond pulse propagation on coplanar striplines fabricated on lossy semiconductor substrates: Modeling and experiments," *IEEE Trans. Microwave Theory Tech.*, vol. 41, pp. 1574–1580, Sept. 1993.
[6] C. R. Paul, *Introduction to Electromagnetic Compatibility*, New York: Wiley, 1992, ch. 13.
[7] R. N. Simons, N. I. Dib, R. Q. Lee, and L. P. B. Katehi, "Modeling of coplanar stripline discontinuities," *IEEE Trans. Microwave Theory Tech.*, vol. 44, pp. 711–716, May 1996.
[8] K. Goverdhanam, R. N. Simons, N. I. Dib, and L. P. B. Katehi, "Coplanar stripline components for high frequency applications," *IEEE Trans. Microwave Theory Tech.*, vol. 45, pp. 1725–1729, Oct. 1997.
[9] K. Goverdhanam, R. N. Simons, and L. P. B. Katehi, "Coplanar stripline propagation characteristics and bandpass filter," *IEEE Microwave Guided Wave Lett.*, vol. 7, pp. 214–216, Aug. 1997.
[10] S.-G. Mao, H.-K. Chiou, and C. H. Chen, "Modeling of lumped-element coplanar stripline low-pass filter," *IEEE Microwave Guided Wave Lett.*, vol. 8, pp. 141–143, Mar. 1998.
[11] V. Trifunović and B. Jokanović, "Review of printed Marchand and double Y baluns: Characteristics and application," *IEEE Trans. Microwave Theory Tech.*, vol. 42, pp. 1454–1462, Aug. 1994.
[12] C.-H. Ho, L. Fan, and K. Chang, "Broad-band uniplanar hybrid-ring and branch-line couplers," *IEEE Trans. Microwave Theory Tech.*, vol. 41, pp. 2116–2125, Dec. 1993.
[13] M. Houdart and C. Aury, "Various excitations of coplanar waveguide," in *IEEE MTT-S Int. Microwave Symp. Dig.*, 1979, pp. 116–118.
[14] J. A. Eisenberg, J. S. Panelli, and W. Ou, "Slotline and coplanar waveguide team to realize a novel MMIC double balanced mixer," *Microwave J.*, pp. 123–131, Sept. 1992.
[15] W. Grammer and K. S. Yngvesson, "Coplanar waveguide transitions to slotline: design and microprobe characterization," *IEEE Trans. Microwave Theory Tech.*, vol. 41, pp. 1653–1658, Sept. 1993.
[16] D. Mirshekar-Syahkal, D. J. Newson, D. Wake, and I. D. Henning, "Wide-band transitions for applications in MMIC's and OEIC's," *IEEE Microwave Guided Wave Lett.*, vol. 4, pp. 299–300, Sept. 1994.
[17] Y.-D. Lin and S.-N. Tsai, "Coplanar waveguide-fed uniplanar bow-tie antenna," *IEEE Trans. Antennas Propagat.*, vol. 45, pp. 305–306, Feb. 1997.
[18] R. Chadha and K. C. Gupta, "Compensation of discontinuities in planar transmission lines," *IEEE Trans. Microwave Theory Tech.*, vol. MTT-30, pp. 2151–2155, Dec. 1982.
[19] C.-T. Hwang and R.-B. Wu, "Partially prizm-gridded FDTD analysis for layered structures of transversely curved boundary," in *IEEE MTT-S Int. Microwave Symp. Dig.*, 1998, pp. 1417–1420.
[20] K. C. Gupta, R. Garg, I. Bahl, and P. Bhartia, *Microstrip Lines and Slotlines*, 2nd ed. Norwood, MA: Artech House, 1996, ch. 5 and 7.
[21] G. Ghione, "A CAD-oriented analytical model for the losses of general asymmetic coplanar lines in hybrid and monolithic MIC's," *IEEE Trans. Microwave Theory Tech.*, vol. 41, pp. 1499–1510, Sept. 1993.
[22] K. Lu, "An efficient method for analysis of arbitary nonuniform transmission lines," *IEEE Trans. Microwave Theory Tech.*, vol. 45, pp. 9–14, Jan. 1997.
[23] S. L. March, "Analyzing lossy radial-line stubs," *IEEE Trans. Microwave Theory Tech.*, vol. 33, pp. 269–271, Mar. 1985.
[24] R. K. Hoffmann, *Handbook of Microwave Integrated Circuits*. Norwood, MA: Artech House, 1987, ch. 14.
[25] J. P. Berenger, "A perfectly matched layer for the absorption of electromagnetic waves," *J. Comput. Phys.*, vol. 114, pp. 185–200, Oct. 1994.

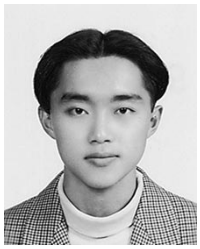

Shau-Gang Mao (S'95) was born in Kaohsiung, Taiwan, R.O.C., on October 11, 1970. He received the B.S. degree in atmosphere science, and the M.S.E.E. and the Ph.D. degrees in electrical engineering from the National Taiwan University, Taipei, Taiwan, R.O.C., in 1992, 1994 and 1998, respectively.

He is currently fulfilling military service in the Department of Communication and Information, Coast Guard Agency of Taiwan, Taiwan, R.O.C., where he is involved in the Coastal Surveillance Wireless Communication and Radar Systems project. His research interests include the design and analysis of RF and microwave circuits and systems.

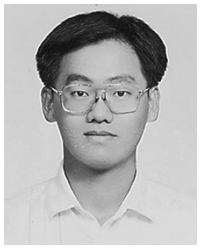

Chieh-Tsao Hwang was born in Tainan, Taiwan, R.O.C., in 1968. He received the B.S. in physics, and the M.S. and Ph.D. degrees in electrical engineering from the National Taiwan University, Taipei, Taiwan, R.O.C., in 1991, 1993 and 1999, respectively.

His areas of interest include computational electromagnetics, transmission-line discontinuities, and electromagnetic theory.

Ruey-Beei Wu (M'91–SM'97) was born in Tainan, Taiwan, R.O.C., in 1957. He received the B.S.E.E. and Ph.D. degrees from the National Taiwan University, Taipei, Taiwan, R.O.C., in 1979 and 1985, respectively.

In 1982, he joined the faculty of the Department of Electrical Engineering, National Taiwan University, where he is currently a Professor. From March 1986 to February 1987, he was a Visiting Scholar at IBM, East Fishkill, NY, and in the Electrical Engineering Department, University of California at Los Angeles, from August 1994 to July 1995. Since 1998, he has been the Director of the National Center for High-Performance Computing, National Science Council, Taiwan, R.O.C. His areas of interest include computational electromagnetics, dielectric waveguides, edge-slot antennas, wave scattering of composite materials, transmission-line discontinuities, and interconnection modeling for computer packaging.

Chun Hsiung Chen (SM'88–F'96) was born in Taipei, Taiwan, R.O.C., on March 7, 1937. He received the B.S.E.E. degree and Ph.D. degree in electrical engineering from the National Taiwan University, Taipei, Taiwan, R.O.C., in 1960 and 1972, respectively, and the M.S.E.E. degree from the National Chiao Tung University, Hsinchu, Taiwan, R.O.C., in 1962.

In 1963, he joined the Faculty of the Department of Electrical Engineering, National Taiwan University, where he is currently a Professor. From August 1982 to July 1985, he was Chairman of the Department of Electrical Engineering at the same university. From August 1992 to July 1996, he was the Director of the University Computer Center. In 1974, he was a Visiting Researcher in the Department of Electrical Engineering and Computer Sciences, University of California at Berkeley. From August 1986 to July 1987, he was a Visiting Professor in the Department of Electrical Engineering, University of Houston, Houston, TX. In 1989, 1990, and 1994, he visited the Microwave Department, Technical University of Munich, Munich, Germany, Laboratoire d'Optique Electromagnetique, Faculte des Sciences et Techniques de Saint-Jerome, Universite d'Aix-Marseille III, France, and the Department of Electrical Engineering, Michigan State University, East Lansing, respectively. His areas of interest include waveguide and component analysis, propagation and scattering of waves, and numerical techniques in electromagnetics.